General methods for the determination of the stiffness tensor and mass density of thin films using Brillouin light scattering: Study of tungsten carbide films

T. Wittkowski,[1] G. Distler,[1] K. Jung,[1] B. Hillebrands,[1] and J. D. Comins[2]
[1]*Fachbereich Physik and Forschungsschwerpunkt MINAS, Technische Universität Kaiserslautern, Erwin-Schrödinger-Strasse 56, D-67663 Kaiserslautern, Germany*
[2]*Materials Physics Research Institute, School of Physics, University of the Witwatersrand, Johannesburg, Wits 2050, South Africa*
(Received 9 July 2003; published 10 May 2004)

Methods of film preparation and data evaluation are presented to determine the stiffness tensor and mass density of thin films using Brillouin light scattering from surface phonons. The combined use of stepped films of progressively increasing thickness d, and an optimized variation of the magnitude of the surface wave vector $q_\parallel$ provides a particularly wide range of uniformly distributed values of the product $q_\parallel d$ in the study of the velocity dispersion of the observed surface acoustic waves. Furthermore by the independent variation of $q_\parallel$ and d, the microstructure can be assessed as a function of film thickness. In the present case of tungsten carbide (WC) films on a silicon substrate, being a slow-on-fast system, the Rayleigh mode and several Sezawa modes are observed. Using the extensive velocity dispersion data, five independent material parameters of the WC films, i.e., four elastic constants and the mass density, are determined by two independent approaches. One employs a least-squares fit to the experimental velocity dispersion curves to determine these material parameters, whereas the other investigates the structure of the parameter space in the vicinity of the solution being sought by a Monte Carlo technique. Both approaches yield identical and self-consistent results. In a Green's-function formulation that uses the vertical displacement component of the acoustic excitations at the free surface, the experimental Brillouin spectra are simulated in the discrete as well as in the continuous part of the mode spectrum.

DOI: 10.1103/PhysRevB.69.205401 PACS number(s): 78.35.+c, 68.60.Bs, 62.20.Dc

I. INTRODUCTION

Brillouin light scattering from surface phonons (known also as surface Brillouin scattering) has emerged in recent years as a favored method to determine the acoustic excitations and elastic properties of thin supported films where the thickness of the film is $\lesssim 1000$ nm.[1–4] Depending on the substrate and film combination, various near-surface excitations can be examined including Rayleigh surface acoustic waves (SAW), Sezawa waves, Love waves, pseudo-SAW, and interface modes. In situations in which the transparency of the film is such that the Brillouin scattering cross section includes contributions from the elasto-optic and ripple mechanisms, sufficiently rich spectral information can be provided so that it is possible to determine the full elastic tensor of the film.[5–7] The process can be aided by the sensitivity of certain elastic constants to particular acoustic excitations. In the case of opaque or near opaque materials, the surface ripple mechanism is dominant and the contributions of elasto-optic scattering are negligibly small which in many cases leads to considerable simplification of the scattering cross section. Theoretical methods including the development of surface Green's function approaches allow the Brillouin spectra and the dispersion of the excitations to be understood in detail and hence provide valuable materials properties such as the film elastic constants, mass density, film thickness, texture, and adhesion. On the other hand film opacity removes the advantages exploited in the studies of near transparent films, *inter alia* of observing shear-horizontal and bulk modes, and limits the possibility of detecting predominantly longitudinally polarized surface modes. Accordingly, methods to determine the full stiffness tensor of opaque thin films have proved elusive and form an important part of the present investigation.

Although Brillouin light scattering from surface modes has been used to investigate the above properties in a wide range of thin films, it is important to distinguish between two distinct situations: ''substrate stiffening'' in which the shear velocity of the film is greater than that of the substrate $v_T^F > v_T^S$ and the presence of the film increases the SAW velocity over that of the substrate (fast-on-slow system) and ''substrate loading'' $v_T^F < v_T^S$ where the converse occurs (slow-on-fast system). In terms of the extraction of the elastic constants, the opaque fast-on-slow systems remain somewhat intractable owing to the limited number of excitations present in such systems. Investigations have thus used a ''forward'' approach in which the Brillouin spectra and dispersion curves have been computationally simulated by making initial assumptions concerning the values of the elastic constants and compared with experimental results. The ''inverse'' process in which the intention is to determine the elastic constants from the measurements has been applied with success to certain slow-on-fast systems. These display, under appropriate conditions, the Rayleigh SAW, and film guided modes known as Sezawa waves whose displacement fields extend throughout the layer and decreases exponentially in the substrate.[8] The conventional method for the determination of the elastic constants is to fit the phase velocity dispersion curves of v versu $q_\parallel d$ where $q_\parallel$ is the magnitude of the parallel surface wave vector and d is the film thickness.

Early studies[9] identified the ambiguities that can result

in the determination of elastic constants by fitting the SAW velocity dispersion curves of leaky excitations. In order to simplify the problem it is therefore useful to analyze the dispersion in the discrete part of the mode spectrum. Since the SAW velocities depend on the various elastic constants to a different extent for the individual modes and for particular $q_{\|}d$ regions, it is attractive to have a large data set extending over a wide range of the dispersion and containing the information of several higher-order modes. Efforts in this direction have analyzed films of different thickness that were deposited under identical conditions.[10–13] It has also been shown that a high precision Brillouin data set, in which attention is given to the determination of sensitive variables such as the film thickness and density, results in the accurate determination of the elastic constants. In addition the mass density may be included as a free fitting parameter.[14,15] In many investigations the constraints of a small $q_{\|}d$ range of the dispersion and a low number of Sezawa modes makes it necessary to restrict the number of free parameters which can be determined from a least squares fit. As a consequence the mass density is usually determined by an independent method and the film properties are assumed to possess high symmetry which in turn justifies the use of an isotropic model. The two independent stiffness constants then act as free parameters.

Furthermore the considerations discussed above are strictly valid only if the film material does not alter its microstructure as a function of the distance from the interface. In many cases transition layers between substrate and film material can occur. In particular, a gradient or a layered substructure is likely to appear if films are deposited in processes which comprise high energies and particle momenta and are thus far from thermodynamical equilibrium. With increasing thickness the film material may even undergo crystallographic phase transitions. These phenomena have been documented unambiguously by Brillouin scattering from surface and interfacial phonons.[16–20] In the present study a special technique of film preparation and measurement allows a detailed examination of the possible variation of the microstructure with film thickness.

At present there is considerable interest in the elastic properties of thin hard films owing to their applications as protective coatings, e.g., in cutting tools. Fast-on-slow conditions prevail in many situations involving opaque hard coatings resulting in the difficulties discussed above in attempts to determine the elastic properties. Of the possible hard coating materials, the widely used tungsten carbide (WC) thin sputtered films provide an attractive case to study since, with their unusually high mass density, they readily fall into the slow-on-fast category of systems if deposited on silicon. See Ref. 21 for a review on the elastic properties of WC.

The electronic properties of single crystal WC (space group $P\bar{6}m2$) lead to a complex chemical bonding situation where the highly localized d orbitals of W create strong covalent W-W bonds, and the nonlocalized electron background is responsible for the electrical conductivity, this being similar to the bonding in W metal. The partly ionic W-C bond is considered to contribute significantly to the observed strength of WC. The C-C bonds are graphitelike and not diamondlike, due to their separation in the WC crystal.[22,23] The large mass density and high melting point, chemical inertness, and electrical conductivity of WC yield other possible fields of application. These include the use of WC films as diffusion barriers for the Al (Ref. 24) or Cu (Refs. 25 and 26) metallization of silicon, the deposition of epitaxial W_2C on MgO (Ref. 27) the preparation of Schottky contacts on 6H-SiC for high-temperature electronic applications,[28] and the protective effect of WC coated walls in fusion reactors.[29,30]

The elastic properties of the WC films measured by Brillouin light scattering are expressed in terms of effective elastic constants, these being averaged over a characteristic length of the order of the phonon wavelength. The hexagonal model in which the c axis is in the direction of the surface normal of the film describes a material of axial symmetry and provides an appropriate description of the elastic properties of most hard coatings including the WC thin films discussed in the present paper. Isotropy prevails in the film plane but anisotropy is allowed in the perpendicular direction.[31,32] The solutions of the equations of motion for the surface modes decouple for solutions with shear-horizontal displacement components. Thus only four of the five independent elastic constants are required to describe these modes. In consequence the elastic properties of the film are expressed in terms of the effective elastic constants c_{11}, c_{13}, c_{33}, c_{55}, and the film density ρ as independent parameters.

WC thin films were grown as 11 sequential thickness steps ranging from 60 to 655 nm on a single crystal silicon substrate during the same growth run. By means of the variation of film thickness and incident angle, a wide range of the product of surface wave vector and thickness ($q_{\|}d$) was available for the study of the velocity dispersion. Furthermore numerous Sezawa modes were observable making the system amenable for the extraction of several material constants. In this context we have used the conventional fitting method discussed above and a new independent method in which a Monte Carlo formulation was used. With the unusually large data set, both approaches allowed five free parameters including the effective elastic constants and the mass density of the WC films to be determined and provided a self-consistent evaluation of these material properties.

II. EXPERIMENTAL ASPECTS

A. Preparation and characterization of the WC thin films

The WC films were grown in a sequence of steps of differing thickness on an unheated crystalline silicon substrate by unbalanced rf magnetron sputtering using a WC target in a pure argon atmosphere at a pressure of 6×10^{-3} mbar. In the unbalanced magnetron configuration the plasma density is increased over an extended region in front of the target so that the substrate at a distance of 60 mm from the target was exposed to an intense ion flux. The equipment and general experimental procedures have been discussed previously.[33]

In order to remove the naturally occurring thin oxide layer (approx 2 nm) on the surface of the silicon substrate, and to

improve film adhesion, the substrate was sputter etched prior to the film deposition process. Special care was taken to ensure that the electric potentials near the substrate surface were not altered during the deposition of the film steps. Accordingly, the substrate was moved behind a fixed window while being maintained at a potential of 0 V. The thinnest intended film layer was deposited first over the entire surface, followed by appropriate movement of the substrate to prevent further deposition in the region of the intended thinnest step while the remaining exposed region was subject to further film growth. This procedure was continued in an undisturbed manner for each of the 11 film steps created until the desired film thickness range of 60–655 nm was achieved. Since the film growth takes place in an uninterrupted fashion within a single growth run, the lateral uniformity of the microstructure of all film steps is ensured.

Two particle fluxes are important for optimal film growth, the flux of film-building W and C atoms and the argon ion flux that densifies the film,[34] the latter being measured with a Faraday cup. With a retarding field, information can be obtained on the mean ion energy and energy spread. For the chosen conditions the measured ion energy of 31 eV corresponds to the potential difference between the plasma and the grounded substrate. The full width at half maximum of the energy distribution was 9 eV and the flux of the singly charged ions onto the substrate was $\Phi_{Ar^+}=0.65$ mA/cm^2. The film growth rate was 0.283 ± 0.005 nm/s and was found to be strictly constant. By assuming no resputtering of the film, the flux ratio of plating and film-building particles was $\Phi_{Ar^+}/(\Phi_W+\Phi_C)=1.8$. Consequently the adatom mobility is decisively affected by the energy and momentum of the impinging ions.

Several analytical techniques were applied in order to characterize the film material as thoroughly as possible. Sputter profiling of the films in combination with Auger-electron spectroscopy confirmed that their composition is homogeneous throughout. Analysis of the carbon to tungsten ratio showed that the WC films are stoichiometric, i.e., possess the same W:C ratio as the target. X-ray-diffraction investigations under grazing incidence revealed that the films deposited in the manner described are predominantly amorphous. However, small nanocrystalline fractions consisting of the cubic β-WC_{1-x} phase and the hexagonal α-W_2C phase cannot be excluded. In a study of a selected surface area of 400×400 nm^2 by scanning tunneling microscopy, the films appeared extremely smooth, exhibiting an rms roughness of 0.36 nm.

Considerable care was taken in the determination of the thickness of the sequence of steps in the deposited film. Several direct measurements were made of the thickness of each such step of the film using a profilometer, taking into account the small correction necessary to account for the depth of the sputter etched regions of the silicon substrate. Each measured film thickness was compared with that calculated from the constant film growth rate and the deposition time. Excellent agreement in the respective film thicknesses was achieved with these two methods.

B. Investigation by surface Brillouin light scattering

Brillouin spectra were excited using an argon ion laser of wavelength $\lambda_i=514.5$ nm operated in a single frequency mode and with the power on the sample being 150 mW. The scattered light was analyzed with a computer-controlled Brillouin spectrometer based on a Sandercock $3+3$ pass tandem Fabry-Pérot interferometer, its intensity being measured with a low noise photo detector. An electromechanical double shutter reduced the intense elastically scattered light thereby protecting the detector while injecting a low intensity reference beam for stabilization of the interferometer transmission. Instruments of this type have been described in the literature.[35] The laser beam was focused onto the sample at room temperature using a lens of focal length 50 mm in a backscattering arrangement. The laser light of wave vector k_i impinges on the sample with angle of incidence Θ (angle between the incident light direction and the normal to the surface) and the light backscattered into a cone is collected by the same lens. The application of energy and wave-vector conservation applied to the Brillouin scattering process involving an acoustic excitation with surface wave vector $q_\parallel$ and angular frequency ω yield the following equations: $q_\parallel=2k_i\sin\Theta=4\pi\sin\Theta/\lambda_i$, and $v=\omega/q_\parallel=\lambda_i\Delta f/2\sin\Theta$, where v is the phase velocity of the surface excitation and Δf is the frequency shift of the scattered light. Measurement errors resulting from the finite aperture[36] were minimized by the use of a slit of width 5 mm, corresponding to an f number of 10.2 for the polar angle.

III. THEORETICAL ASPECTS

WC films are opaque and as discussed above, the scattered Brillouin intensity is dominated by the surface ripple mechanism. At room temperature and above where $T\gg\hbar\omega/k_B$, the surface Brillouin scattering efficiency for this mechanism is proportional to the power spectrum of the normal displacements of the surface with that wave vector and at that frequency. The power spectrum is related to G_{33}, the (x_3,x_3) component of the Fourier (frequency and wave vector) domain elastodynamic Green's function evaluated at the surface $(x_3=-d)$. Thus

$$I(\omega)\propto A\frac{T}{\omega}\mathrm{Im}\{G_{33}(q_\parallel,x_3=-d,\omega+i0)\}, \qquad (1)$$

where A depends on the properties of the medium, the scattering geometry, and the frequency and polarization of the incident light. The details of the calculation of G_{33}, in terms of the partial waves that satisfy the boundary conditions at the free surface and the film-substrate interface for a thin homogeneous film of thickness d, are given by Zhang *et al.*[37] The complete surface Brillouin spectrum is simulated, giving the usually intense discrete modes (true surface waves) as well as the higher-frequency weak continuum of excitations resulting from the surface displacements of the bulk waves and within which pseudosurface waves, having partial waves with a bulklike character, and damped resonances may have an appreciable scattering intensity.

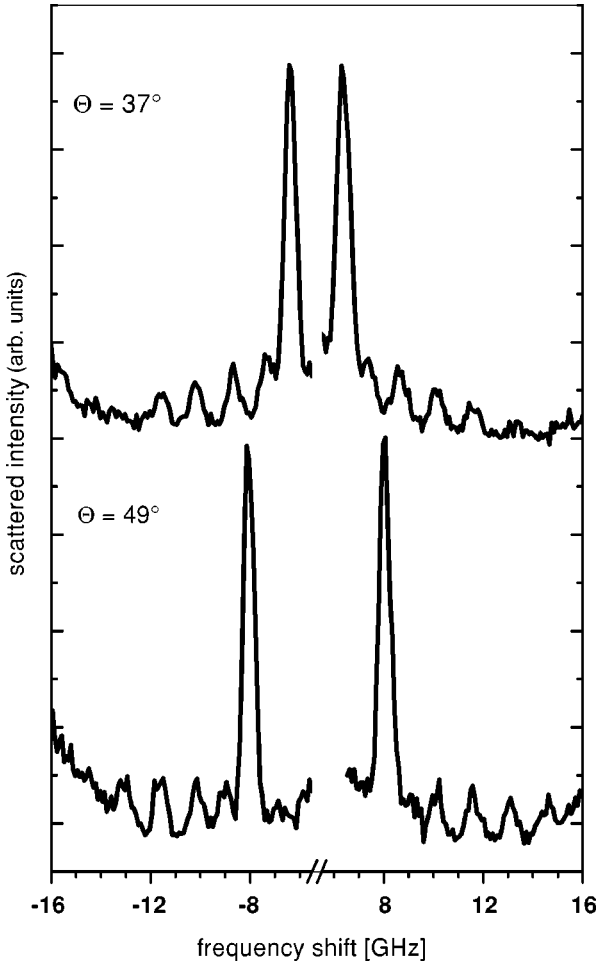

FIG. 1. Representative measured Brillouin spectra for the variation of $q_{\|}d$ by changing the angle of incidence for the WC film of thickness 595 nm. Spectra are relatively displaced for ease of observation. The lower spectrum corresponds to $q_{\|}=18.43\ \mu\mathrm{m}^{-1}$ while in the upper spectrum $q_{\|}=14.70\ \mu\mathrm{m}^{-1}$. In addition to the velocity dispersion the frequencies shift $\propto \sin\Theta$. The elastic peaks in each spectrum are removed for clarity.

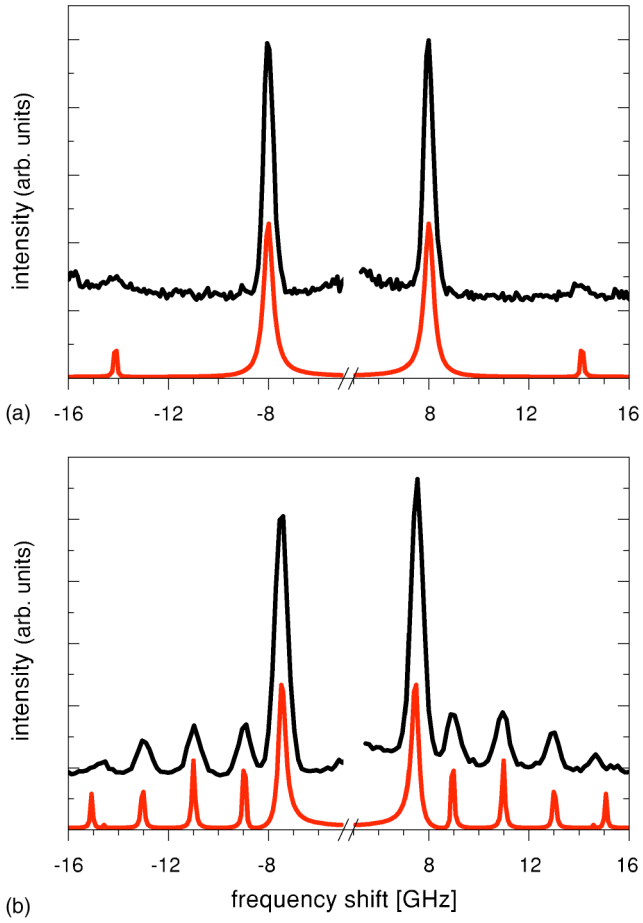

FIG. 2. (a) Measured and calculated Brillouin spectra for the WC film of thickness $d=60$ nm with $q_{\|}=17.47\ \mu\mathrm{m}^{-1}$ yielding $q_{\|}d=1.04$. The calculated spectrum uses the elastic constant values determined from the fitting of the dispersion curves. Spectra are relatively displaced for ease of observation; the elastically scattered peaks are removed. (b) Measured and calculated Brillouin spectra for the WC film of thickness $d=417$ nm with $q_{\|}=17.27\ \mu\mathrm{m}^{-1}$ yielding $q_{\|}d=7.20$. The calculated spectrum uses the elastic constant values determined from the fitting of the dispersion curves. Spectra are relatively displaced for ease of observation; the elastically scattered peaks are removed. The frequencies and the relative intensities of different modes, corresponding to the areas under their peaks, are well reproduced by the calculation. The peaks corresponding to the fourth and fifth Sezawa mode in (b) are not well resolved in the experimental spectrum. As can be presumed from Fig. 4 their intensity ratio is very sensitive to small variations in the film parameters in this region of the mode spectrum.

IV. RESULTS

In Fig. 1 two representative measured surface Brillouin spectra are shown for the film of thickness 595 nm in which the surface wave vector $q_{\|}$ is, respectively, 14.70 and 18.43 $\mu\mathrm{m}^{-1}$. Inelastic scattering peaks from the Rayleigh and several Sezawa modes are present. The strong elastically scattered peak around 0 GHz is removed for clarity.

Figure 2 shows Brillouin spectra for films of thickness 60 and 417 nm, respectively, for a value of $q_{\|}=17.27\ \mu\mathrm{m}^{-1}$. These are representative of the spectra for low values of $q_{\|}d$ in which only one Sezawa mode is observed besides the Rayleigh mode [Fig. 2(a)] and spectra for high values of $q_{\|}d$ where numerous Sezawa modes are seen [Fig. 2(b)].

The SAW phase velocity dispersion with $q_{\|}d$ for the various film steps over the complete range of film thickness of the sample is shown in Fig. 3. The homogeneity of the films and the precision of the thickness measurements also permit a precise match with additional data provided by the variation of $q_{\|}$ by a change in the angle of incidence Θ for two film steps near the beginning and end of the range. It is seen from the figure that with the extended range of film thickness and the numerous Sezawa waves, a particularly large data set consisting of 87 measured points is achieved.

A weighted least-squares fit of the velocity dispersion curves using as free parameters the effective elastic constants c_{11}, c_{13}, c_{33}, c_{55}, and the film density ρ was performed involving the minimization of

$$\chi^2=\sum_{j=1}^{21}\sum_{i} w_{ij}(v_{ij}^{(meas)}-v_{ij}^{(cal)})^2, \qquad (2)$$

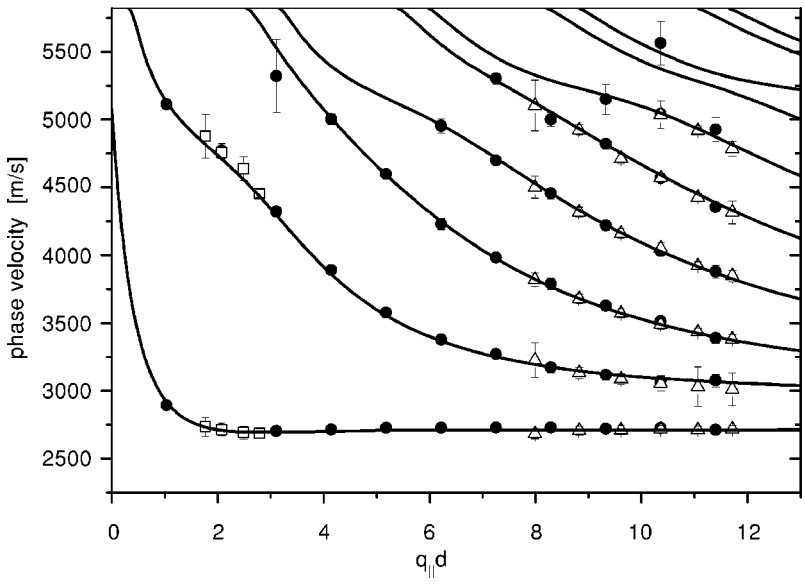

FIG. 3. Phase velocity dispersion curves for the discrete sagittally polarized surface waves (Rayleigh and Sezawa) as a function of $q_{\parallel}d$ in which the filled circles represent measurements made with a constant $q_{\parallel}$ value of 17.27 μm^{-1} over the complete range of film thickness. For two film steps of thickness 191 nm (open squares) and 595 nm (open triangles) the value of $q_{\parallel}$ was varied. Each method used in the determination of $q_{\parallel}d$ results in the same velocity dispersion. The lines represent the computed best fit to the experimental data.

where the right sum is performed over all mode velocities for a particular value of $q_{\parallel}d$ and i is less or equal to 6. The left sum runs over all values of $q_{\parallel}d$, thus covering a wide range of the SAW dispersion as documented in Fig. 3. The weighting factors w_{ij} were determined from the individual measurement errors. The phase velocities were calculated by solving the equation of motion under the appropriate boundary conditions.[8] Except for one point the assignment of the measured velocities to the correct mode order was unambiguous, so that 86 data points could be used in the fitting routine. From the best fit, the resulting effective elastic constants for the WC film material were determined as $c_{11}=349\pm7$ GPa, $c_{13}=126\pm8$ GPa, $c_{33}=348\pm13$ GPa, and $c_{55}=114\pm2$ GPa and the film density as $\rho=13.0\pm0.2$ g/cm^3. The $\chi^2_{\min}$ sum of 20.24, divided by the number of degrees of freedom (81) is 0.25, indicating an excellent reliability of the fit. The near equality of c_{11} and c_{33}, and the values of the anisotropy factors, namely, $A_1=c_{11}/c_{33}=1.002$ and $A_2=2c_{55}/(c_{11}-c_{13})=1.019$, justify the assumption of an essentially isotropic film. Accordingly the value of c_{12} may be determined by setting $c_{12}=c_{13}$. Thus, in this case, the complete elastic tensor is determined together

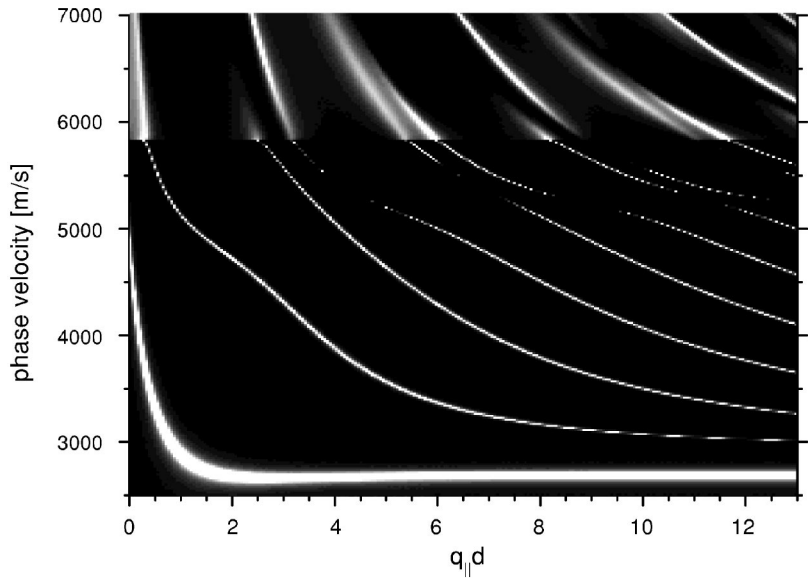

FIG. 4. Brillouin intensities calculated by the elastodynamic Green's function using the G_{33} component. The calculated spectra use the elastic constant values determined from the fitting of the dispersion curves. Displayed intensities are normalized for the discrete and the continuous ($v>5822$ m/s) mode spectrum and for each value of $q_{\parallel}d$. Due to the opacity of the film the Brillouin intensities are dominated by the surface ripple mechanism which is proportional to the power spectrum of the vertical displacement component at the free surface. The low intensities observed around $v=5178$ m/s for $q_{\parallel}d>4$ is due to the mainly longitudinal character of partial waves and corresponds to the longitudinal sound velocity of the material parallel to the film. The presence of several damped resonant excitations in the continuous spectrum is shown. These latter characteristics are also emphasized in Fig. 5.

with the density from the measurements. Hence, the bulk modulus of the WC film material is $B=\frac{1}{3}(c_{11}+2c_{12})=200 \pm 8$ GPa.

The evaluation of the G_{33} component of the Green's function at the free surface yields the scattered mode intensities for a given value of $q_{\|}d$, as shown in Fig. 4. In the discrete part of the spectrum the low intensity in the velocity region for $q_{\|}d>4$ around the longitudinal sound velocity parallel to the film, $v_{L,\|}^{film}=\sqrt{c_{11}/\rho}=5178$ m/s, is due to predominantly longitudinal displacement components at the free surface for certain modes at that velocity. Furthermore it is noted from Fig. 4 that there are damped resonances of measurable intensity predicted within the continuum of excitations beyond the transonic state. With the optimal choice of the free spectral range (FSR) of the interferometer for the observation and measurement of the discrete Rayleigh and Sezawa modes, such resonances were not observed in the experimental spectra as they appear in the same spectral region as the tails of the more intense "ghost peaks" arising from the transmission function of the tandem interferometer. However, such resonances were observed in additional measurements by an appropriate enlargement of the FSR. In Fig. 5 examples of resonances (being identified from Fig. 4) are shown in the experimental spectra for $q_{\|}d=4.64$ and $q_{\|}d=2.46$. They are distinctly broader than the sequence of Sezawa mode peaks. Figure 5(a) consistently shows the absence of the third Sezawa mode in the experimental as well as in the computed spectrum for a particular value of $q_{\|}d$.

In a separate approach a Monte Carlo method was used to evaluate the effective elastic constants and the mass density. Starting from the experimental data shown in Fig. 3 new data sets, also consisting of 86 data points, were generated by a random variation of quintuplets of the free parameters, the c_{ij} and ρ, within specified intervals. The weighted χ^2-sum for each data set was computed according to Eq. (2). This approach is appropriate to determine the absolute and relative minima of an objective function (i.e., the χ^2 sum) in a multidimensional or complex-structured parameter space. It is stressed that this Monte Carlo method is a stand-alone procedure that only requires the experimental data as input. It is thus not necessary to select a particular starting set of parameters, e.g., from a fit to experimental results or from the literature, and investigate the parameter space around this point. Since, however, the previously described deterministic fitting algorithm converged satisfactorily in determining the minimum in the χ^2 sum, we concentrated our statistical analysis on the parameter space surrounding of the absolute minimum $\chi^2_{\min}$. Figures 6 and 7 present the results of 7.5×10^8 randomly chosen and evaluated data sets. Computation time on a modern personal computer CPU at a processing frequency of 1.8 GHz was approximately 1 week. The computation can be distributed on several CPU's to ensure that the time frames are shorter.

Figures 6(a)–6(c) show projections of the parameter space onto the (c_{11},c_{33})-, the (c_{33},c_{13})-, and the (c_{55},ρ)-plane for the free parameter quintuplets with χ^2 in the vicinity of $\chi^2_{\min}$. Among the ten two-dimensional subspaces these three chosen planes represent the parameter

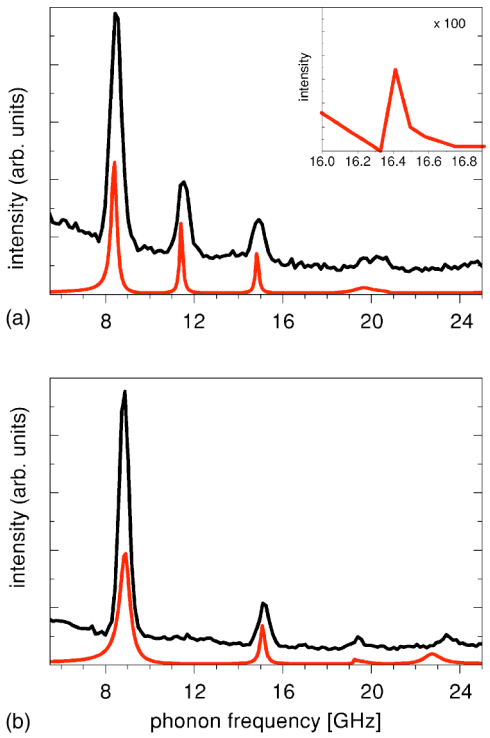

FIG. 5. Measured and calculated Brillouin spectra for the WC film of thickness $d=238$ nm with $q_{\|}=19.51$ μm^{-1} yielding $q_{\|}d=4.64$ shown in (a), and $d=119$ nm with $q_{\|}=20.71$ μm^{-1} yielding $q_{\|}d=2.46$ shown in (b). The calculated spectra use the values of the elastic constants determined from the fitting of the dispersion curves. Spectra are relatively displaced for ease of observation. Spectrum (a) illustrates the near absence of the third Sezawa mode resulting from its extremely small vertical displacement components. The computed spectrum for the relevant spectral region is shown magnified in the inset. The presence of damped resonances above 18.08 GHz (a) and 19.19 GHz (b) in the continuum of excitations is observable due to the enlarged FSR. The agreement between measured and computed spectra is good except for the frequency of the resonance at approximately 23 GHz in spectrum (b). This discrepancy could not be reduced by a slight variation of parameters nor by including additional Green's tensor components in the computation, thus its origin remains obscure. The appearance of sharp resonances could be used in general to deduce stiffness constants in a fitting routine. This is of special advantage in the event of insufficient velocity data from discrete modes.

pairs which are the most strongly correlated. Projections of different sets of points show areas that are related to different values of $\Delta\chi^2$, where $\Delta\chi^2=\chi^2-\chi^2_{\min}$. These diagrams emphasize the parameter correlation and provide an insight into the structure of the parameter space. An analysis of the probability distribution functions of the individual parameters shows that these are not normally distributed in general so that the results shown in Fig. 6 provide an appropriate presentation of the parameter space for chosen values of $\Delta\chi^2$. Figure 7 shows the Monte Carlo results of the weighted sum of squares for the two anisotropy factors A_1 and A_2 of the film material. Starting from the hexagonal symmetry model, the smallest χ^2 sum clearly corresponds to nearly isotropic parameters.

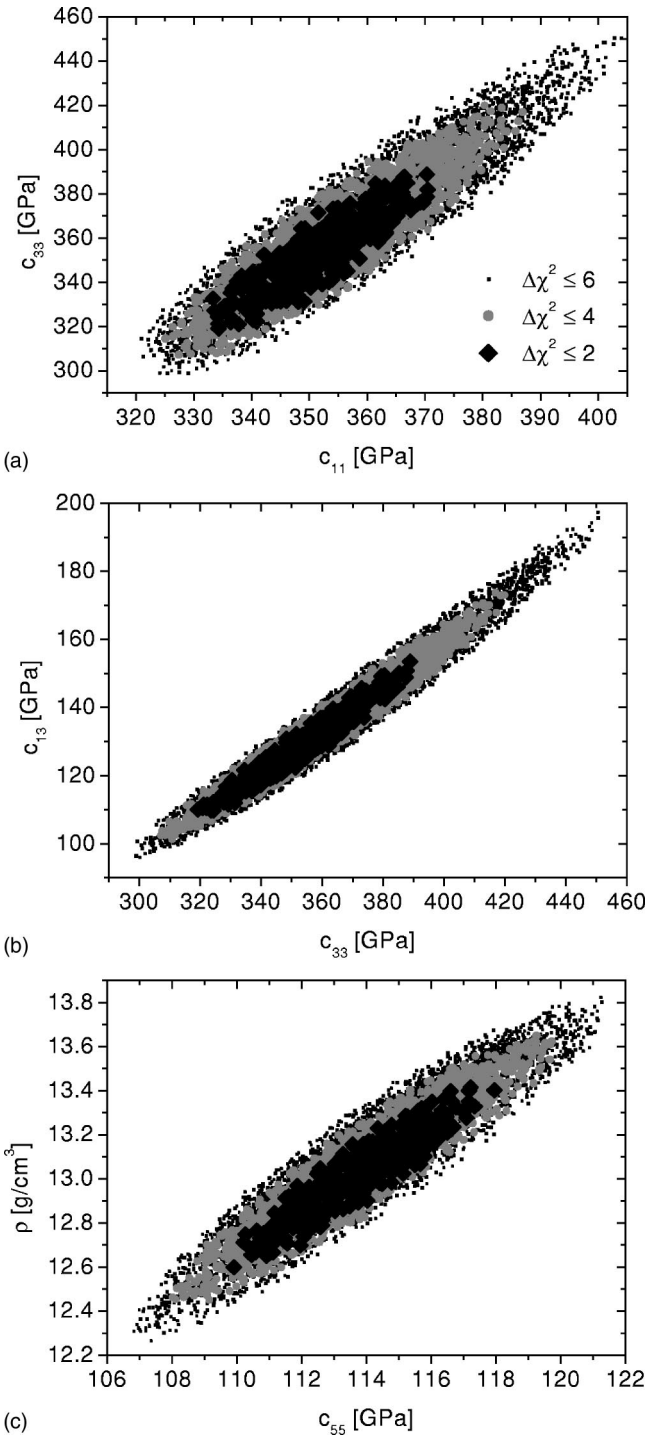

FIG. 6. Projections of the parameter space onto the (c_{11},c_{33})-, the (c_{33},c_{13})-, and the (c_{55},ρ)-plane for the quintuplets of free parameters with χ^2 in the vicinity of $\chi^2_{\min}$. The three chosen planes represent the parameter pairs which are most strongly correlated. Projections of different sets of points show areas that are related to different values of $\Delta\chi^2$, where $\Delta\chi^2=\chi^2-\chi^2_{\min}$. The constant c_{13}, which usually is difficult to determine due to its strong correlation with the other constants, is quantified with fair accuracy.

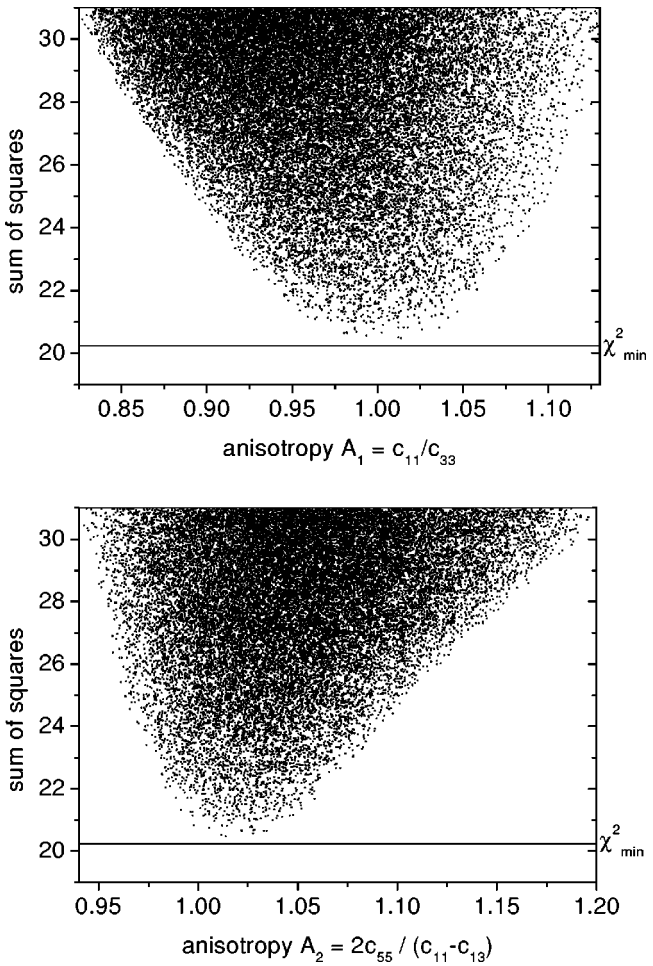

FIG. 7. Monte Carlo results of the weighted sum of squares for the two anisotropy factors A_1 and A_2 of the film material. Starting from the hexagonal symmetry model, the smallest χ^2 sum clearly corresponds to nearly isotropic parameters for this type of film. The straight line in both diagrams indicates the minimum χ^2 sum that was obtained with the least-squares fit.

V. DISCUSSION

The method of film growth developed in the present study is shown to be particularly well suited to the needs of Brillouin scattering investigations where the velocity dispersion of acoustic surface modes is used to determine the materials properties of the film. With the deposition technique used, numerous film steps of different thickness are prepared within an individual sample in one deposition run, thus avoiding alterations in the deposition conditions that may appear if the deposition is interrupted. Hence it is a relatively simple matter to produce the large velocity dispersion data sets required for the successful extraction of the elastic constants and the mass density. Since the velocities of the various SAW modes are sensitive to a different extent on these individual materials parameters for particular $q_\parallel d$ ranges, Brillouin measurements on stepped films provide the necessary database even if the parameter sensitivity is unknown. The ability to independently vary the surface phonon wave vector and film thickness allows one to assess whether the film material is homogeneous leading to a single set of elastic constants or if its properties vary with film thickness.

This deposition method has been illustrated using stepped WC films on a silicon substrate. Although WC is a hard

material, its high mass density results in a slow-on-fast situation in which in addition to the Rayleigh SAW, numerous Sezawa modes are observed facilitating the determination of the elastic properties of the film. Two methods have been used to determine the set of effective elastic constants using a hexagonal symmetry model, namely, a least-squares fitting of the velocity dispersion curves and a newly developed Monte Carlo approach in which the results achieved by the minimization procedure are examined statistically. While both methods in which the four elastic constants and the mass density of the film were used as free parameters yielded self-consistent results, the Monte Carlo technique provides additional information on the structure of the parameter space. Both techniques revealed a near isotropy of the WC film material and a growth behavior which is independent from the distance to the interface. From earlier investigations it is known that the microstructure of WC films depends critically on their deposition conditions.[34] Preliminary results of the velocity dispersion of the Rayleigh-like modes with Brillouin light scattering show a pronounced elastic anisotropy of the films if the ion energy is increased.[40]

Finally, the material parameters obtained from the present study are discussed and interpreted in relation to available single-crystal data. The lower mass density of 13.0 g/cm^3 for the films compared with the value of $\rho = 15.62$ g/cm^3 for a hexagonal tungsten monocarbide single crystal calculated with the lattice constants of Ref. 38, is typical for amorphous materials and is in accord with the possible presence of microvoids. Effective elastic constants of an aggregate of randomly oriented WC crystals deduced from the Voigt and Reuss averages and using the only available single crystal values of hexagonal tungsten monocarbide from Ref. 39, are $c_{11} = 815 \pm 10$ GPa, $c_{12} = 251 \pm 1$ GPa, $c_{55} = 282 \pm 4$ GPa, and hence $B = 439.5 \pm 5$ GPa. The error in the polycrystal aggregate values is half the difference of the results of both averaging methods. Although, due to the different microstructure of the aggregate, these values are not directly comparable to the film constants determined in the present study, the general behavior of a stiffness reduction of the amorphous film material due to enlarged bond lengths and due to the possible presence of microvoids is observed. A more detailed analysis will be provided in Ref. 40.

VI. CONCLUSION

General methods of film preparation and data evaluation have been presented for the determination of the full stiffness tensor and the mass density of thin films from Brillouin scattering experiments. The new elements of these techniques, namely, the preparation of stepped films thus yielding a large database and the use of a statistical approach to determine material parameters and to investigate the parameter space, are generally applicable not only to opaque films and Rayleigh-like modes. They are also potentially important for the analysis of fast-on-slow situations, transparent films, and acoustic modes of different character, e.g., shear-horizontal modes and interfacial modes. The capability of these methods has been demonstrated on tungsten carbide films where five independent parameters of this opaque material were determined exclusively from the dispersion of SAW's in conjunction with an appropriate theoretical model assuming hexagonal symmetry and thus avoiding the uncertainties inherent in the often-used isotropic model. With these parameters experimental Brillouin spectra were satisfactorily synthesized by a Green's-function technique.

ACKNOWLEDGMENTS

J.D.C. wishes to express his gratitude to the Deutscher Akademischer Austauschdienst—DAAD and the South African National Research Foundation for financial support. He also wishes to thank the group AG Hillebrands for the kind hospitality during his visit to the University of Kaiserslautern. The authors thank Dr. M. Scheib and D.M. Woll both at the Institut für Oberflächen- und Schichtanalytik GmbH, TU Kaiserslautern for the XRD and AES analysis as well as Dr. M. Rickart for the scanning tunnel microscope measurements. Financial support by the Deutsche Forschungsgemeinschaft is gratefully acknowledged.

[1] G.I. Stegemann and F. Nizzoli, in *Surface Excitations*, edited by V.M. Agranovich and R. Loudon (Elsevier, Amsterdam/North-Holland, Amsterdam, 1984), Chap. 2, pp. 195–378.

[2] F. Nizzoli and J.R. Sandercock, in *Dynamical Properties of Solids*, edited by G.K. Horton and A.A. Maradudin (Elsevier, Amsterdam/North-Holland, Amsterdam, 1990), Chapter 5, pp. 281–335.

[3] P. Mutti, C.E. Bottani, G. Ghislotti, M. Beghi, G.A.D. Briggs, and J.R. Sandercock, in *Advances in Acoustic Microscopy*, Vol. 1, edited by A. Briggs (Plenum, New York, 1995), Chapter 7, pp. 249–300.

[4] J.D. Comins, in *Handbook of Elastic Properties of Solids, Liquids, and Gases*, edited by M. Levy, H.E. Bass, and R.R. Stern, *Vol. I: Dynamic methods for measuring the elastic properties of solids*, edited by A.G. Every and W. Sachse (Academic, New York, 2001), Ch. 15, pp. 349–378.

[5] V. Panella, G. Carlotti, G. Socino, L. Giovannini, M. Eddrief, K. Amimer, and C. Sébenne, J. Phys.: Condens. Matter **9**, 5575 (1997).

[6] F. Nizzoli, B. Hillebrands, S. Lee, G.I. Stegeman, G. Duda, G. Wegner, and W. Knoll, Phys. Rev. B **40**, 3323 (1989).

[7] G. Carlotti, D. Fioretto, G. Socino, and E. Verona, J. Phys.: Condens. Matter **7**, 9147 (1995).

[8] G.W. Farnell and E.L. Adler, in *Physical Acoustics*, edited by W.P. Mason and R.N. Thurston (Academic, New York, 1972), Vol. 9, pp. 35–127.

[9] F. Nizzoli, R. Bhadra, O.F. de Lima, M.B. Brodsky, and M. Grimsditch, Phys. Rev. B **37**, 1007 (1988).

[10] S. Lee, B. Hillebrands, G.I. Stegeman, H. Cheng, J.E. Potts, and F. Nizzoli, J. Appl. Phys. **63**, 1914 (1988).

[11] T. Wittkowski, J. Jorzick, K. Jung, and B. Hillebrands, Thin Solid Films **353**, 137 (1999).

[12] V. Panella, G. Carlotti, G. Socino, L. Giovannini, M. Eddrief, and C. Sébenne, J. Phys.: Condens. Matter **11**, 6661 (1999).
[13] W. Pang, A.G. Every, J.D. Comins, P.R. Stoddart, and X. Zhang, J. Appl. Phys. **86**, 311 (1999).
[14] B. Hillebrands, P. Baumgart, R. Mock, G. Güntherodt, and P.S. Bechthold, J. Appl. Phys. **58**, 3166 (1985).
[15] M.G. Beghi, C.E. Bottani, P.M. Ossi, T.A. Lafford, and B.K. Tanner, J. Appl. Phys. **81**, 672 (1997).
[16] A.G. Every, W. Pang, J.D. Comins, and P.R. Stoddart, Ultrasonics **36**, 223 (1998).
[17] T. Wittkowski, P. Cortina, J. Jorzick, K. Jung, and B. Hillebrands, Diamond Relat. Mater. **9**, 1957 (2000).
[18] T. Wittkowski, V. Wiehn, J. Jorzick, K. Jung, and B. Hillebrands, Thin Solid Films **368**, 216 (2000).
[19] P. Zinin, M.H. Manghnani, X. Zhang, H. Feldermann, C. Ronning, and H. Hofsäss, J. Appl. Phys. **91**, 4196 (2002).
[20] X. Zhang and R. Sooryakumar, Appl. Phys. Lett. **80**, 4501 (2002).
[21] C. Kral, W. Lengauer, D. Rafaja, and P. Ettmayer, J. Alloys Compd. **265**, 215 (1998).
[22] V.P. Zhukov and V.A. Gubanov, Inorg. Mater. **22**, 1665 (1986).
[23] A.Y. Liu, R.M. Wentzcovitch, and M.L. Cohen, Phys. Rev. B **38**, 9483 (1988).
[24] S. Ghaisas, J. Appl. Phys. **70**, 7626 (1991).
[25] Y.-M. Sun, S.Y. Lee, A.M. Lemonds, E.R. Engbrecht, S. Veldman, J. Lozano, J.M. White, J.G. Ekerdt, I. Emesh, and K. Pfeifer, Thin Solid Films **397**, 109 (2001).
[26] S.J. Wang, H.J. Tsai, S.C. Sun, and M.H. Shiao, J. Electrochem. Soc. **148**, G500 (2001).
[27] U. Jansson, H. Högberg, J.-P. Palmquist, L. Norin, J.O. Malm, L. Hultman, and J. Birch, Surf. Coat. Technol. **142**, 817 (2001).
[28] N. Lundberg, M. Östling, C.-M. Zetterling, P. Tägström, and U. Jansson, J. Electron. Mater. **29**, 372 (2000).
[29] T. Horikawa, B. Tsuchiya, and K. Morita, J. Nucl. Mater. **258**, 1087 (1998).
[30] K. Morita and K. Soda, J. Nucl. Sci. Technol. **39**, 344 (2002).
[31] B.A. Auld, *Acoustic Fields and Waves in Solids* (Wiley, New York, 1979), Vol. 1.
[32] T. Wittkowski, J. Jorzick, K. Jung, B. Hillebrands, M. Keunecke, and K. Bewilogua, J. Appl. Phys. **91**, 2729 (2002).
[33] G. Keller, I. Barzen, R. Erz, W. Dötter, S. Ulrich, K. Jung, and H. Ehrhardt, Fresenius' J. Anal. Chem. **341**, 349 (1991).
[34] G. Keller, I. Barzen, W. Dötter, R. Erz, S. Ulrich, K. Jung, and H. Ehrhardt, Mater. Sci. Eng., A **139**, 137 (1991).
[35] B. Hillebrands, Rev. Sci. Instrum. **70**, 1589 (1999).
[36] P.R. Stoddart, J.C. Crowhurst, A.G. Every, and J.D. Comins, J. Opt. Soc. Am. B **15**, 2481 (1998).
[37] X. Zhang, J.D. Comins, A.G. Every, P.R. Stoddart, W. Pang, and T.E. Derry, Phys. Rev. B **58**, 13 677 (1998).
[38] L.E. Toth, *Transition Metal Carbides and Nitrides* (Academic, New York, 1971).
[39] M. Lee and R.S. Gilmore, J. Mater. Sci. **17**, 2657 (1982).
[40] T. Wittkowski, G. Distler, K. Jung, B. Hillebrands, J.D. Comins, Appl. Phys. Lett. (to be published).